Relation between Supramolecular Order and Charge Carrier Mobility of Branched Alkyl Hexa-*peri*-hexabenzocoronenes

Wojciech Pisula,[†] Marcel Kastler,[†] Daniel Wasserfallen,[†] Mihail Mondeshki,[†] Jorge Piris,[‡] Ingo Schnell,[†] and Klaus Müllen*,[†]

Max-Planck-Institute for Polymer Research, Ackermannweg 10, D-55128 Mainz, Germany, and Radiation Chemistry Department, IRI, Delft University of Technology, Mekelweg 15, NL-2629 JB Delft, The Netherlands

Received January 30, 2006. Revised Manuscript Received June 2, 2006

The control of the solubility and thermal behavior of discotic materials requires a variation of the substituents. In this study, it has been shown that long alkyl side chains branched at the very close vicinity of a hexa-*peri*-hexabenzocoronene (HBC) aromatic core results in the decrease of the π interaction between single disks and thus in a significant lowering of the isotropization temperature but maintains a high degree of intracolumnar order at room temperature, which is usually the operating temperature in electronic devices. The pronounced molecular packing yielded one of the highest charge carrier mobilities obtained for a noncrystalline discotic compound giving these materials importance as attractive organic semiconductors for organic electronics. This stands in strong contrast to the behavior of other large discotic molecules substituted by bulky alkyl side chains; they generally lead to an increase of the intracolumnar disorder which is a disadvantage for the one-dimensional charge carrier transport.

1. Introduction

A focus in the ongoing quest for miniaturization of electronic devices is on the organization of molecules on the nanometer scale.[1] The fundamental idea is to engineer the chemical composition and the intermolecular interactions of the individual building blocks such that the self-organized system exhibits the desired properties.[2] A major challenge in this context is to elucidate the relationship between chemical structure, morphology, and the device performance.

In the past two decades, discotic liquid crystalline (LC) materials have attracted considerable interest because of their unique self-organization behavior into columnar superstructures, leading to high charge carrier mobilities along the columnar stacks.[3] This feature resulted in a successful application of such materials in field-effect transistors and photovoltaic devices.[4] Hexa-*peri*-hexabenzocoronenes (HBCs) are particularly promising because their large aromatic core permits one of the highest values for the intrinsic charge carrier mobility for mesogenes.[5]

Further prerequisites for an efficient charge carrier transport between electrodes are a high purity of the material, to reduce possible trapping sites for charge carriers, and a pronounced and defect-free long-range order. For device fabrication, it is necessary to control the orientation of the disklike molecules with respect to the substrate or electrodes.[4a,6] Appropriate processing techniques, such as Langmuir−Blodgett,[7] or solution casting onto pre-oriented PTFE substrates,[8] were applied to form uniaxially, macroscopically oriented surface layers. Zone-processing techniques such as solution based zone casting[9] and zone crystallization[10] from the isotropic state were both successfully applied. The self-assembly of the material, tuned by changing the chemical nature of the substituents in the corona of the HBC disk, defined the processibility and the alignment techniques.

* Corresponding author. E-mail: muellen@mpip-mainz.mpg.de. Tel.: (+49) 6131 379 150. Fax: (+49) 6131 379 350. E-mail: muellen@mpip-mainz.mpg.de.
† Max-Planck-Institute for Polymer Research.
‡ Delft University of Technology.

(1) (a) Sirringhaus, H.; Tessler, N.; Friend, R. H. *Science* **1998**, *280*, 1741. (b) Chen, J.; Reed, M. A.; Rawlett, A. M.; Tour, J. M. *Science* **1999**, *286*, 1550. (c) Duan, X.; Niu, C.; Sahi, V.; Chen, J.; Parce, J. W.; Empedocles, S.; Goldman, J. L. *Nature* **2003**, *425*, 274.

(2) (a) Brunsveld, L.; Folmer, B. J. B.; Meijer, E. W.; Sijbesma, R. P.; *Chem. Rev.* **2001**, *101*, 4071. (b) Ciferri, A. *Makromol. Chem. Rapid Commun.* **2002**, *23*, 511. (c) Bong, D. T.; Clark, T. D.; Granja, J. R.; Ghadiri, M. R. *Angew. Chem., Int. Ed.* **2001**, *40*, 988.

(3) (a) Boden, N.; Bushby, R. J.; Clements, J.; Movaghar, B.; Donovan, K. J.; Kreouzis, T. *Phys. Rev. B* **1995**, *52*, 13274. (b) Adam, D.; Schuhmacher, P.; Simmerer, J.; Haussling, L.; Siemensmeyer, K.; Etzbach, K. H.; Ringsdorf, H.; Haarer, D. *Nature* **1994**, *371*, 141. (c) Eichhorn, H. *J. Porphyrins Phthalocyanines* **2000**, *4*, 88.

(4) (a) Pisula, W.; Menon, A.; Stepputat, M.; Lieberwirth, I.; Kolb, U.; Tracz, A.; Sirringhaus, H.; Pakula, T.; Müllen, K. *Adv. Mater.* **2005**, *17*, 684. (b) Schmidt-Mende, L.; Fechtenkötter, A.; Müllen, K.; Moons, E.; Friend, R. H.; MacKenzie, J. D. *Science* **2001**, *293*, 1119.

(5) (a) van de Craats, A. M.; Warman, J. M.; Fechtenkötter, A.; Brand, J. D.; Harbison, M. A.; Müllen, K. *Adv. Mater.* **1999**, *11*, 1469. (b) Warman, J. M.; van de Craats, A. M. *Mol. Cryst. Liq. Cryst.* **2003**, *396*, 41.

(6) (a) Bao, Z. N.; Lovinger, A. J.; Dodabalapur, A. *Adv. Mater.* **1997**, *9*, 42. (b) Noh, Y.-Y.; Kim, J.-J.; Yoshida, Y.; Yase, K. *Adv. Mater.* **2003**, *15*, 699. (c) Bunk, O.; Nielsen, M. M.; Solling, T. I.; van de Craats, A. M.; Stutzmann, N. *J. Am. Chem. Soc.* **2003**, *125*, 2252.

(7) (a) Tsukruk, V. V.; Wendorff, J. H.; Karthaus, O.; Ringsdorf, H. *Langmuir* **1993**, *9*, 614. (b) Karthaus, O.; Ringsdorf, H.; Tsukruk, V. V.; Wendorff, J. H. *Langmuir* **1992**, *8*, 2279. (c) Laursen, B. W.; Norgaard, K.; Reitzel, N.; Simonsen, J. B.; Nielsen, C. B.; Als-Nielsen, J.; Bjornholm, T.; Solling, T. I.; Nielsen, M. M.; Bunk, O.; Kjaer, K.; Tchebotareva, N.; Watson, M. D.; Müllen, K.; Piris, J. *Langmuir* **2004**, *20*, 4139. (d) Reitzel, N.; Hassenkam, T.; Balashev, K.; Jensen, T. R.; Howes, P. B.; Kjaer, K.; Fechtenkötter, A.; Tchebotareva, N.; Ito, S.; Müllen, K.; Bjornholm, T. *Chem.−Eur. J.* **2001**, *7*, 4894.

(8) (a) Zimmermann, S.; Wendorff, J. H.; Weder, C. *Chem. Mater.* **2002**, *14*, 2218. (b) van de Craats, A. M.; Stutzmann, N.; Bunk, O.; Nielsen, M. M.; Watson, M.; Müllen, K.; Chanzy, H. D.; Sirringhaus, H.; Friend, R. H. *Adv. Mater.* **2003**, *15*, 495. (c) Piris, J.; Debije, M. G.; Stutzmann, N.; van de Craats, A.; Watson, M. D.; Müllen, K.; Warman, J. M. *Adv. Mater.* **2003**, *15*, 1736.

10.1021/cm0602343 CCC: $33.50
Published on Web 07/12/2006

Besides the control of the thermal behavior and the solubility, it is desirable for material processing to tune the supramolecular self-organization and thus the growth. A lowering of the isotropization temperatures below the thermal decomposition threshold allows processing from the melt. The control of the thermal behavior of HBCs, however, requires the variation of substituents, which are able to influence sterically the π interaction between the aromatic core leading to columnar breaking at lower temperatures. Various examples in the literature have proven that this leads to a significantly lower intracolumnar ordering which in turn limits the charge carrier mobility of the material as reported for molecules consisting of a larger disk.[11] Side chain bearing functionalities revealed an enhanced flexibility and increased also the space-filling requirements of the substituents as observed recently for various HBC derivatives, but also in these cases, the higher ordered phases were reached only below 0 °C.[12]

It is of fundamental interest for the design of new organic semiconductors not only to control the long-range organization but also to increase the nanoscopic order between single building blocks. Because the operating temperature is mainly the room temperature, it is desired to obtain a high intermolecular interaction accompanied by an improved packing of the molecules at ambient conditions. Additionally, these materials should be processible from the melt or from solution. Both aspects including processibility and high supramolecular order have not been regarded intensively enough for discotic compounds in materials science.

Recently, we have reported the effect of linear and branched alkyl substituents on the self-organization of HBCs (Figure 1) in solution and in solution processed films.[13] It has been shown that both features important for device fabrication, the significant lowering of the isotropization temperature and the pronounced self-assembly, are controlled in a straightforward way. The increased intracolumnar order at room temperature was accompanied by high charge carrier mobility. Herein, the effects induced by a distinct variation of the length and thus of the steric demand of side chains in the corona of the HBC core (Figure 1, compounds **1**−**3**) are investigated with respect to their thermal behavior, the nanoscopic self-organization, and the charge carrier mobility.

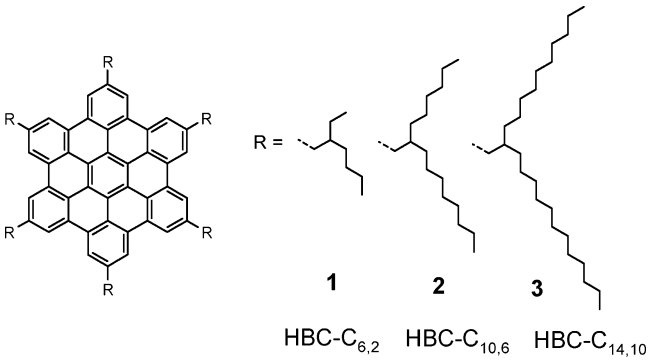

Figure 1. Chemical structures of HBC−$C_{6,2}$ **1**, HBC−$C_{10,6}$ **2**, and HBC−$C_{14,10}$ **3**.

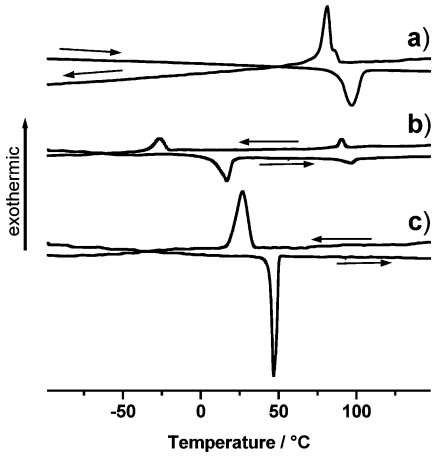

Figure 2. DSC traces of (a) HBC−$C_{6,2}$ **1**, (b) HBC−$C_{10,6}$ **2**, and (c) HBC−$C_{14,10}$ **3** (arrows indicate heating/cooling directions).

Table 1. Thermal Characterization for the Investigated Dovetailed HBC Derivatives 1−3[a]

sample	temperature, °C	enthalpy, kJ mol^{-1}	phase transition
HBC−$C_{6,2}$ **1**	97 (81)	25.3 (20.5)	C_r−Col_d
	420 (380)[b]		Col_d−I
HBC−$C_{10,6}$ **2**	17 (−26)	27.5 (14.8)	Col_p−Col_d
	97 (91)	4.7 (4.7)	Col_d−I
HBC−$C_{14,10}$ **3**	46 (26)	92.5 (91.9)	Col_p−I

[a] Abbreviations: C_r = crystalline phase, Col_p = plastic crystalline, Col_d = columnar disordered LC, and I = isotropic phase. Parantheses indicate values during cooling. [b] Above thermal decomposition, assigned with POM by rapid heating.

2. Thermal Behavior

The thermal behavior was determined for all three compounds HBC−$C_{6,2}$ (**1**), HBC−$C_{10,6}$ (**2**), and HBC−$C_{14,10}$ (**3**) by using differential scanning calorimetry (DSC) in the temperature range from −150 °C to 220 °C (2 °C/min; Figure 2), whereby the phase characterization was based on results from polarized optical microscopy (POM), solid-state NMR, and X-ray diffraction. As expected, a strong influence of the alkyl substituents on the thermal behavior was observed (Table 1).

Compound HBC−$C_{6,2}$ **1** exhibited one phase transition at 97 °C upon heating from the crystalline phase to the LC state, which appeared at 81 °C during cooling (Figure 2a).

(9) (a) Tracz, A.; Jeszka, J. K.; Watson, M. D.; Pisula, W.; Müllen, K.; Pakula, T. *J. Am. Chem. Soc.* **2003**, *125*, 1682. (b) Tracz, A.; Pakula, T.; Jeszka, J. K. *Mater. Sci.* **2004**, *22*, 415. (c) Piris, J.; Pisula, W.; Tracz, A.; Pakula, T.; Müllen, K.; Warman, J. *Liq. Cryst.* **2004**, *31*, 993. (d) Piris, J.; Debije, M. G.; Stutzmann, N.; Laursen, B. W.; Pisula, W.; Watson, M. D.; Bjornholm, T.; Müllen, K.; Warman, J. M. *Adv. Funct. Mater.* **2004**, *14*, 1053. (e) Piris, J.; Pisula, W.; Warman, J. M. *Synth. Met.* **2004**, *147*, 85. (f) Pisula, W.; Tomovic, Z.; Stepputat, M.; Kolb, U.; Pakula, T.; Müllen, K. *Chem. Mater.* **2005**, *17*, 2641. (g) Breiby, D. W.; Bunk, O.; Pisula, W.; Sølling, T. I.; Tracz, A.; Pakula, T.; Müllen, K.; Nielsen, M. M. *J. Am. Chem. Soc.* **2005**, *127*, 11288. (h) Breiby, D. W.; Hansteen, F.; Pisula, W.; Bunk, O.; Kolb, U.; Andreasen, J. W.; Müllen, K.; Nielsen, M. M. *J. Phys. Chem. B* **2005**, *109*, 22319.

(10) (a) Liu, C. Y.; Bard, A. J. *Chem. Mater.* **2000**, *12*, 2353. (b) Pisula, W.; Kastler, M.; Wasserfallen, D.; Pakula, T.; Müllen, K. *J. Am. Chem. Soc.* **2004**, *126*, 8074.

(11) (a) Gearba, R. I.; Bondar, A. I.; Goderis, B.; Bras, W.; Ivanov, D. A.; *Chem. Mater.* **2005**, *17*, 2825. (b) Komatsu, T.; Ohta, K.; Watanabe, T.; Ikemoto, H.; Fujimoto, T.; Yamamoto, I. *J. Mater. Chem.* **1994**, *4*, 537. (c) Bryant, G. C.; Cook, M. J.; Haslam, S. D.; Richardson, R. M.; Ryan, T. G.; Thorne, A. J. *J. Chem. Mater.* **1994**, *4*, 209. (d) Ban, K.; Nishizawa, K.; Ohta, K.; van de Craats, A. M.; Warman, J. M.; Yamamotoa, I.; Shiraia, H. *J. Mater. Chem.* **2001**, *11*, 321.

(12) Pisula, W.; Tomovic, Z.; El Hamaoui, B.; Watson, M. D.; Pakula, T.; Müllen, K. *Adv. Funct. Mater.* **2005**, *15*, 893.

(13) Kastler, M.; Pisula, W.; Wasserfallen, D.; Pakula, T.; Müllen, K. *J. Am. Chem. Soc.* **2005**, *127*, 4286.

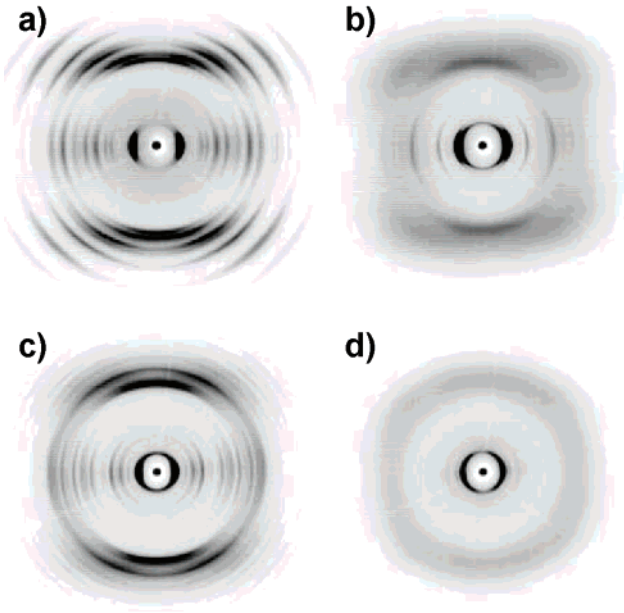

Figure 3. 2D-WAXS pattern of filament extruded of HBC−$C_{6,2}$ **1** (a) in the crystalline and (b) in the LC phase and HBC−$C_{10,6}$ **2** (c) in the plastic crystalline and (d) in the LC phase at 60 °C.

By POM, HBC−$C_{6,2}$ **1** was entering its isotropic state at about 420 °C. In contrast, HBC−$C_{10,6}$ **2** and HBC−$C_{14,10}$ **3** were considered as "plastic crystalline" because of their plastic deformation at room temperature in comparison to crystalline materials such as HBC−$C_{6,2}$ **1**. Additionally, HBC−$C_{14,10}$ **3** exhibited increased side chain dynamics at ambient conditions, confirming this consideration. The DSC trace of HBC−$C_{10,6}$ **2** revealed a transition to the LC phase at 17 °C and at melting point at 97 °C during heating (Figure 2b). HBC−$C_{14,10}$ **3** showed a phase transition directly from the plastic crystalline phase to the isotropic state at 46 °C during heating. The crystallization temperature was observed at 26 °C.

3. Investigation of the Supramolecular Structure by X-ray Diffraction

The relation between molecular structure and the supramolecular organization has been investigated by temperature-dependent two-dimensional wide-angle X-ray scattering (2D-WAXS) and powder X-ray diffraction. The samples for 2D-WAXS experiments were prepared by filament extrusion.[14]

The distinct equatorial reflections in the 2D-WAXS pattern of the compounds **1**−**3** suggested a well-ordered supramolecular structure of the macroscopically oriented filaments with columns aligned along the extrusion direction. The high degree of order for HBC−$C_{6,2}$ **1** and HBC−$C_{10,6}$ **2** was obvious from the large number of higher order reflections in the room-temperature patterns (Figure 3a,c). For all three investigated HBCs, the off-meridional reflections indicated an identical tilt of the discotic cores with respect to the columnar axis with an intracolumnar period of 0.48 nm leading to a "herringbone" structure.[15] The large number of higher order off-meridional reflections of HBC−$C_{6,2}$ **1** implied strong intra- as well intercolumnar correlations between the disks. A tilting disk angle of about 40° with respect to the columnar axis was determined from the reflections with the strongest intensity. Contrary to HBC−$C_{10,6}$ **2** and HBC−$C_{14,10}$ **3**, where the corresponding phase was assigned to a plastic-crystalline phase due to plasticity and a slightly lower long-range correlation, HBC−$C_{6,2}$ **1** formed a crystalline phase at room temperature. A smaller tilting angle of about 25° was found for the HBC−$C_{10,6}$ **2** and HBC−$C_{14,10}$ **3** molecules. The distribution of the equatorial reflections in the 2D-WAXS patterns corresponded to the lateral intercolumnar arrangement.

The intracolumnar order of HBC−$C_{6,2}$ **1** and HBC−$C_{10,6}$ **2** underwent a significant change when heating above the first transition as seen from the 2D-WAXS patterns (Figure 3b,d) typical for a LC phase. With increasing temperature, the meridional reflections corresponding to the disk-to-disk distance for HBC−$C_{10,6}$ **2** faded until they completely disappeared at a temperature of 50 °C, indicating a significant decrease of the intracolumnar order in the higher temperature LC phase. For HBC−$C_{6,2}$ **1**, the X-ray pattern showed that the discs maintained a tilted intracolumnar arrangement of an identical angle but with a significantly lower degree of order than in the crystalline phase. Therefore, for both compounds the higher temperature was identified as a columnar, disordered phase, Col_d. After cooling back to room temperature and annealing at ambient conditions the initial structure of HBC−$C_{6,2}$ **1** and HBC−$C_{10,6}$ **2** was recovered.

The intercolumnar arrangement of the materials in different phases was investigated using powder X-ray scattering. However, the complex diffractograms and the high crystallinity at room temperature complicated the determination of a two-dimensional lateral unit cell characterizing the intercolumnar organization. A lateral monoclinic model was found to give the best fits for the room temperature diffractograms, whereby the unit cell parameters were strongly dependent on the length of the side chains.

The large number and high intensity of sharp reflections observed in the diffractogram of HBC−$C_{6,2}$ **1** confirmed the high crystallinity and the pronounced long-range order of the material. Specifically, the intensive reflections in the wide-angle range (2−3 nm^{-1}) emphasized again the high degree of intracolumnar order (Figure 4a). A similar degree of order was found for HBC−$C_{10,6}$ **2** (Figure 5a) and HBC−$C_{14,10}$ **3** in the plastic crystalline phase, whereby the number of reflections was slightly smaller. Upon heating HBC−$C_{6,2}$ **1** (Figure 4b) and HBC−$C_{10,6}$ **2** (Figure 5b) to the Col_d phase, a considerable structural change occurred, accompanied by the disappearance of most reflections. Surprisingly, in both cases the columnar arrangement in this phase could not be assigned to a hexagonal lattice, which was unusual for C_6-symmetric HBCs. As a result of the tilted packing of the disks, a monoclinic unit cell for HBC−$C_{6,2}$ **1**

(14) Pisula, W.; Tomovic, Z.; Simpson, C.; Kastler, M.; Pakula, T.; Müllen, K. *Chem. Mater.* **2005**, *17*, 4296.

(15) (a) Fischbach, I.; Pakula, T.; Minkin, P.; Fechtenkötter, A.; Müllen, K.; Spiess, H. W.; Saalwächter, K. *J. Phys. Chem. B* **2002**, *106*, 6408. (b) Pisula, W.; Kastler, M.; Wasserfallen, D.; Robertson, J. W. F.; Nolde, F.; Kohl, C.; Müllen, K. *Angew. Chem., Int. Ed.* **2006**, *45*, 819.

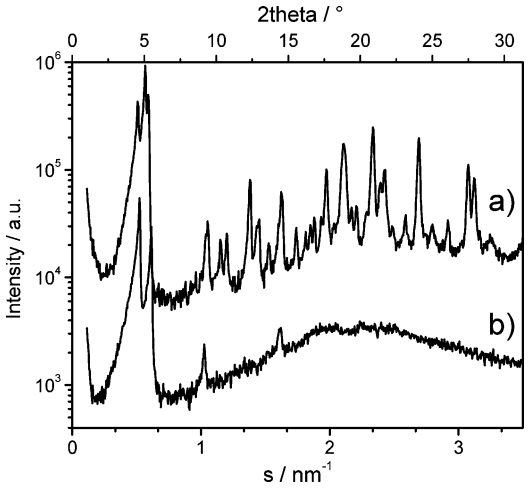

Figure 4. Powder X-ray diffraction of HBC−$C_{6,2}$ **1** at (a) room temperature in the crystalline phase and (b) in the mesophase.

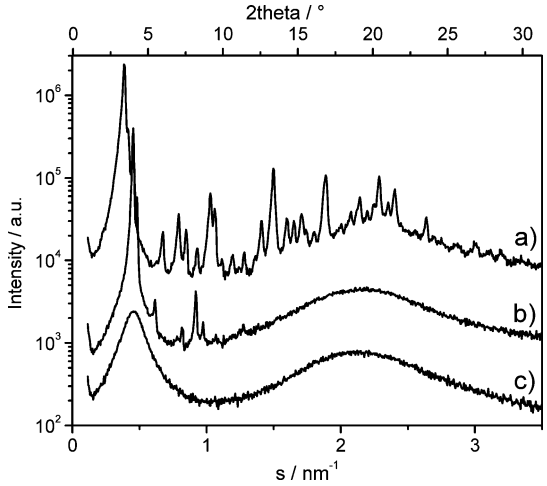

Figure 5. Powder X-ray diffraction of HBC−$C_{10,6}$ **2** at (a) room temperature in the plastic crystalline phase, (b) in the Col_d LC state, and (c) in the isotropic phase.

and an orthorhombic unit cell for HBC−$C_{10,6}$ **2** unit cell were fitted. However, it has been shown that a lattice assignment on the basis of only one powder X-ray diffractogram is misleading in most of the cases. Therefore, additional scattering techniques are needed to verify these results.[6c] Nevertheless, as implied by the high intensity of the split small-angle reflections, a well-ordered intercolumnar packing was maintained. On the contrary, the reflections corresponding to the molecular stacking disappeared, which supported the 2D-WAXS results.

While heating HBC−$C_{10,6}$ **2** to the optically isotropic state, a broad small-angle reflection appeared, corresponding to a periodicity of 2.2 nm as derived from the X-ray diffraction (Figure 5c). This reflection was attributed to a position correlation of molecular aggregates which exhibited a contrast of electron density between the aromatic core stacks and the substituents. From this relation, an average of about three HBC−$C_{10,6}$ **2** molecules was determined with a relatively broad distribution, suggesting that the molecules were not monomeric in the isotropic state but formed aggregates consisting of several disks. The stacking number of four disks for HBC−$C_{14,10}$ **3** was calculated from the X-ray scattering pattern recorded for the isotropic state.

4. Molecular Dynamics and Intracolumnar Stacking by Solid-State NMR

^{1}H magic-angle spinning (MAS) and ^{1}H−^{1}H double-quantum (DQ) MAS NMR experiments were conducted to probe the type of columnar packing of the HBC derivatives in their crystalline states. The ^{1}H−^{1}H DQ MAS spectra revealed typical NMR signal patterns (Figure 6a) arising from a tilted arrangement of the HBC disks, which was also referred to a "herringbone"-type packing. One- and two-dimensional ^{1}H−^{1}H DQ spectra exhibited three distinct resonances of the aromatic protons situated in the "bays" of the HBC cores, which were known to arise from the packing and different π-electron densities as experienced by the aromatic protons.[16] When heating the samples to the respective transition temperatures into the mesophase, the HBC molecules underwent a reorientation from the tilted to a planar arrangement and started a rapid rotation around their columnar axis. In the ^{1}H MAS spectra, this transition manifested itself in the narrowing of the resonance lines. Moreover, the three distinct aromatic peaks observed in the solid state merged into a single aromatic ^{1}H resonance.

The molecular dynamics of the HBC derivatives were investigated by means of sideband patterns observed in ^{1}H−^{13}C rotor-encoded rotational echo double resonance (REREDOR) NMR experiments performed under fast MAS conditions. The experiments yielded local dynamic order parameters (S), which represented the residual motional anisotropy of a given molecular segment.

For alkyl side chains attached to rigid groups or backbones, a mobility gradient was expected, and while the α-CH_2 group should be almost as rigid as the core, the ω-CH_3 group should exhibit the highest mobility (Figure 6b).

For corresponding molecular segments of HBC−$C_{6,2}$ **1** and HBC−$C_{10,6}$ **2**, similar dynamic order parameters were found in the crystalline and plastic crystalline phase, which confirmed the expectations of a relatively rigid aromatic core and more mobile side chains. In the case of HBC−$C_{6,2}$ **1**, the alkyl chain segment mobility gradually increased from the anchoring point ($S \sim 0.7$) at the core toward the chain ends ($S \sim 0.5$, see Figure 6b), while a more uniform chain mobility was determined for HBC−$C_{10,6}$ **2** with a similar regional order of ∼0.65 along the chain. For HBC−$C_{14,10}$ **3**, again a pronounced mobility gradient was found, but the overall chain mobility ($S \sim 0.5 \rightarrow 0.15$ at 16 °C) was significantly higher than in HBC−$C_{10,6}$ **2** and HBC−$C_{6,2}$ **1**.

When heating to the LC state, the fast disk rotation decreased the ^{1}H−^{13}C dipole−dipole couplings in the aromatic CH groups by a factor of 2, as long as the rotation axis paralleled the columnar axis and both were perpendicular to the HBC core plane.[17] Comparing the dynamic order parameter of the cores in the LC phase, HBC−$C_{10,6}$ **2** exhibited the most stable disk rotation with a maximum out-of-plane excursion of ∼24°, which was identical to the tilting angle in the plastic crystalline phase as determined

(16) (a) Brown, S.; Schnell, I.; Brand, J.; Müllen, K.; Spiess, H. W. *J. Am. Chem. Soc.* **1999**, *121*, 6712. (b) Brown, S.; Schnell, I.; Brand, J.; Müllen, K.; Spiess, H. W. *J. Mol. Struct.* **2000**, *521*, 179.
(17) Schnell, I. *Prog. Nucl. Magn. Reson. Spectrosc.* **2004**, *45*, 145.

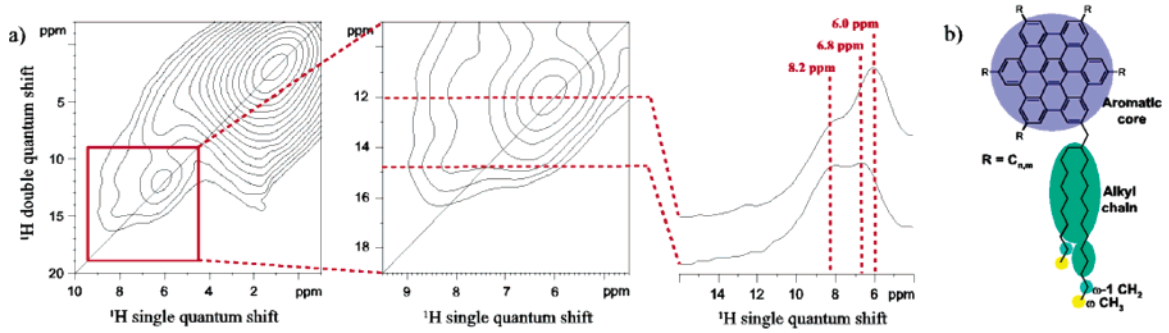

Figure 6. (a) Two-dimensional solid-state ^{1}H−^{1}H DQ MAS NMR spectrum of HBC−$C_{6,2}$ **1** (left) with the aromatic region magnified (middle) and two one-dimensional slices cut at 12.0 and 14.8 ppm (right). The experimental conditions were T = 40 °C, MAS at 25 kHz, and dipolar recoupling (BABA sequence) for one rotor period to excite and reconvert the DQ coherences. (b) Degree of mobility as found by NMR experiments in different parts of the dovetailed HBC derivatives (the blue color displays the rigid HBC core with increasing mobility along the chain to the most mobile regions displayed in yellow): R, dove tail; *n*, number of carbons in the main chain; and *m*, number of carbons in the β chain.

Table 2. Intracolumnar Charge Carrier Mobilities for the Dovetailed HBC Derivatives

sample	phase	$\sum\mu_{1D}$, cm^2 V^{-1} s^{-1}
HBC−$C_{6,2}$ **1**	C_r	0.25
	Col_d	0.29
HBC−$C_{10,6}$ **2**	Col_p	0.73
	Col_d	0.08
HBC−$C_{14,10}$ **3**	Col_p	0.47

by 2D-WAXS. At the same time, HBC−$C_{6,2}$ **1** showed a less stable rotation, as reflected by ∼42° out-of-plane excursion being also in a very good agreement with the structural X-ray analysis, while HBC−$C_{14,10}$ **3** underwent a practically direct transition from the solid phase into the melt, such that there was no well-defined LC phase to be studied.

5. Charge Carrier Mobility

The charge transport properties of the presented branched HBC derivatives were studied by the pulse-radiolysis time-resolved microwave conductivity (PR-TRMC) technique. Pulse irradiation of compounds **1**−**3** resulted in very long-lifed conductivity transients, relative to other HBC derivatives studied before.[18] This was evidence not only for the long-range intracolumnar order but also for the high purity of the materials as a result of their high solubility and, hence, ease of purification.

From the end-of-pulse conductivity the sum of the intracolumnar charge carrier mobilities, $\sum\mu_{1D}$, has been determined as a function of temperature. The values obtained for the different phases are summarized in Table 2. The temperature behavior of the present compounds differed notably from that of the previously studied HBC derivatives;[5b] in general, the mobility increases slightly with temperature in the crystalline phase until it experiences a sudden decrease by a factor of about 2 on entering the mesophase. Most HBC derivatives showed a similar $\sum\mu_{1D}$ value of about 0.3 cm^2/(V s) in their columnar hexagonal mesophases. In contrast, the mobility of 0.3 cm^2/(V s) for HBC−$C_{6,2}$ **1** did not experience any significant change when going from the crystalline to the LC phase.

Figure 7 represents the temperature behavior of the intracolumnar charge carrier mobility for HBC−$C_{10,6}$ **2**. The room-temperature value $\sum\mu_{1D}$ = 0.73 cm^2/(V s) was the highest measured for a noncrystalline phase and was only overcome by the crystalline tetradecyl substituted derivative (HBC−C_{14}; $\sum\mu_{1D}$ = 1.00 cm^2/(V s)).[5a] Upon heating the mobility decreased almost linearly with temperature until it experienced a sudden drop of almost an order of magnitude upon conversion to the LC phase.

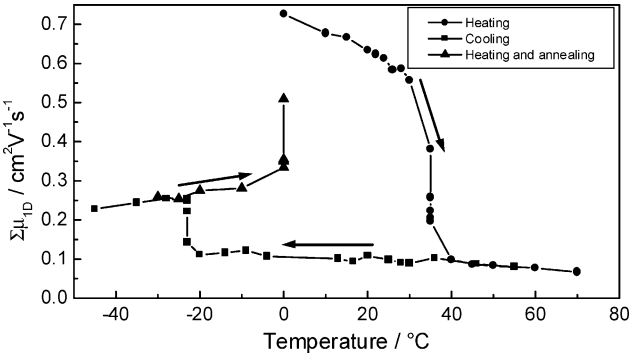

Figure 7. Temperature dependence of the one-dimensional mobility for the first heating (full circles), cooling (open circles), and final heating back to room temperature (full triangles) for the dovetailed HBC−$C_{10,6}$ **2**.

Compound HBC−$C_{14,10}$ **3** was also plastic crystalline at room temperature and accordingly showed a mobility value comparable to the crystalline HBC derivatives.

6. Discussion

In our previous work, we have studied the aggregation behavior in solution of the new branched HBC derivatives HBC−$C_{6,2}$ **1**, HBC−$C_{10,6}$ **2**, and HBC−$C_{14,10}$ **3**. It has been shown that the introduction of the space-filling dovetailed side chains strongly decreased the π stacking of the disks in solution.[13]

The solid-state NMR experiments revealed that the core and chain mobilities in the crystalline or plastic crystalline state were quite similar for HBC−$C_{6,2}$ **1** and HBC−$C_{10,6}$ **2** with a "cone-shaped" mobility gradient of the chain starting from the core toward the ends. On the other hand, HBC−$C_{14,10}$ **3** exhibited even in the plastic crystalline state a high chain mobility due to its length. A slight temperature increase resulted in extremely high dynamics of the tetradecyln-decyl ($C_{14,10}$) side chains and finally in the breaking of the columnar structures leading to the isotropic phase. For HBC−$C_{10,6}$ **2** the isotropization was reached at slightly higher temperatures of 97 °C. Both examples are in contrast to linear

(18) Warman, J. M.; Piris, J.; Pisula, W.; Kastler, M.; Wasserfallen, D.; Müllen, K. *J. Am. Chem. Soc.* **2005**, *127*, 14257.

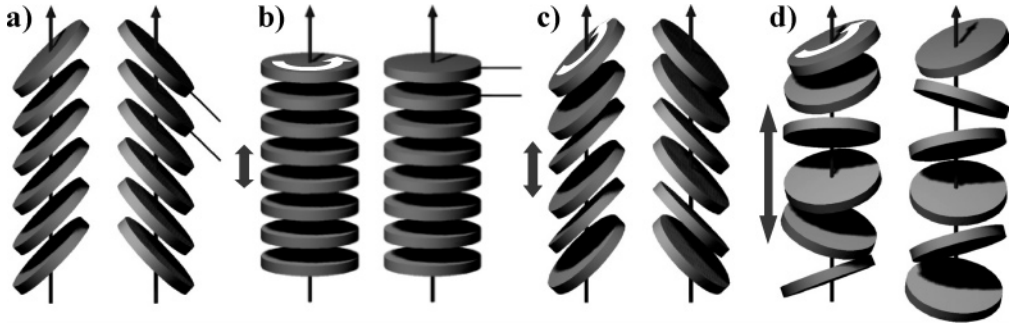

Figure 8. Schematic illustration of the arrangement of the aromatic core in (a) the herringbone order, (b) the planar arrangement which is the characteristic mesophase organization for HBCs substituted by alkyl chains with a low steric demand, and (c) the disordered columnar arrangement of the HBC−$C_{6,2}$ **1** and (d) of the HBC−$C_{10,6}$ **2** disks in the mesophase. The disks possess a rapid rotation around the columnar axes, whereby the longitudinal fluctuations increase with longer side chains.

alkyl substituted derivatives, where the isotropization temperature was not reached before 400 °C. Certainly, the branching site close to the aromatic core bears steric demand during the assembly and resulted in a suppression of the mesophase for HBC−$C_{14,10}$ **3** and in a direct melting from the plastic crystalline phase. The investigation of the thermal behavior indicated that the introduction of a high steric demand can lower efficiently the phase transitions and open the opportunity for the melt processing.

Solid-state NMR and X-ray diffraction experiments were conducted to gain insight into the influence of the side chains on both the macro- and nanoscopic levels. At room-temperature, the phase of HBC−$C_{6,2}$ **1**, HBC−$C_{10,6}$ **2**, and HBC−$C_{14,10}$ **3** revealed a high degree of order confirmed by the X-ray scattering results. The herringbone arrangement was verified for all investigated compounds by both solid-state NMR and X-ray experiments (Figure 8a). In comparison to other discotics substituted by bulky alkoxy side chains possessing a relatively low isotropization temperature, a high intracolumnar organization at ambient temperatures is quite exceptional as other discotics show an ordered columnar phase far below 0 °C. The reason for the pronounced intracolumnar packing might be the crystallization of the purely hydrocarbon alkyl chains at ambient temperatures due to sufficient rigidity. The introduction of functional groups containing oxygen atoms would increase the chain flexibility but lower the intracolumnar order.[12] On the other hand, the heating of HBC−$C_{6,2}$ **1** and HBC−$C_{14,10}$ **2** to the mesophase resulted in the increase of the intracolumnar disorder because of the higher dynamics of the resulting bulkiness of the side chains, which was pronounced for HBC−$C_{10,6}$ **2**. Together with the value for the out-of-plane motion, it became clear that the disklike molecules were 24° arranged with respect to the columnar axis and bounced on top of each other (Figure 8d), which led to a fading of the π-stacking reflection in the X-ray diffractogram. On the other hand, the shorter chains in HBC−$C_{6,2}$ **1** did not prevent the core from approaching but caused a wobbling of the disks, leading to the appearance of the intracolumnar correlation in the X-ray pattern for the mesophase. The solid-state NMR experiments verified the out-of-plane excursion of about 42°, which was identical to the tilting angle in the crystalline phase (Figure 8c). As a result of this asymmetric shape of the columns, both HBC−$C_{6,2}$ **1** and HBC−$C_{10,6}$ **2** did not reveal a hexagonal intercolumnar arrangement in the LC phase, which was atypical for symmetrically 6-fold substituted HBCs. In contrast to the pronounced order in the room temperature phases, the columnar mesophases at elevated temperatures revealed a significant degree of disorder. This behavior was exceptional, especially when compared to HBC derivatives where linear alkyl substituents were introduced.[14,15]

The PR-TRMC measurements provided information about the charge carrier mobility in different phases and were correlated with results described for the columnar packing. The one-dimensional charge carrier transport of HBC−$C_{10,6}$ **2** was strongly dependent on the intracolumnar order and the molecular packing. Disorder resulted in a lowering of the mobility as observed for the LC phase of this compound. In the highly ordered phases, however, HBC−$C_{10,6}$ **2** and HBC−$C_{14,10}$ **3** yielded exceptionally long lifetimes of charges and charge carrier mobilities comparable with highly crystalline HBCs. Identical mobility values for a noncrystalline discotic phase were only observed for lutetium phthalocyanine dimers, as a result of to a small intermolecular distance of 0.33 nm.[19] The two features, long lifetime and high mobility of charges, are important requirements for the application of these HBC derivatives in electronic devices and make them very attractive as organic semiconductors.

7. Conclusions

The introduction of bulky and space-filling alkyl side chains has opened the opportunity to tune the thermal behavior and the solubility over a broad range. In general, the steric demand in the close proximity to the aromatic core is one key to modulate the intermolecular interactions. In this study, it was possible to design HBC molecules with a significantly lowered isotropization temperature maintaining a pronounced intracolumnar packing at room temperature. This is a great advantage in comparison to other discotic HBC derivatives with a low isotropization temperature substituted by bulky side chains which in many cases reveal their higher ordered phases far below room temperature.[12] Because HBC−$C_{10,6}$ **2** exhibited the highest charge carrier mobility for a noncrystalline discotic, this well-ordered material became even more interesting as organic semiconductors for electronic devices and is currently being tested in devices. On the other hand, the solid-state NMR and X-ray

(19) Ban, K.; Nishizawa, K.; Ohta, K.; van de Craats, A. M.; Warman, J. M.; Yamamotoa, I.; Shiraia, H. *J. Mater. Chem.* **2001**, *11*, 321.

results proved that the high dynamics of the bulky substituents at higher temperatures increased the intracolumnar disorder which in turn hindered the one-dimensional migration of charge carriers along these columnar structures.

The straightforward synthetic route allowing a facile tailoring of the bulk properties and the thermal processing accompanied by a high charge carrier mobility are two aspects which are fundamental for the fabrication of low-cost organic electronics.

8. Experimental Section

The synthesis of HBC−$C_{6,2}$ **1**, HBC−$C_{10,6}$ **2**, and HBC−$C_{14,10}$ **3** has been described elsewhere.[13]

DSC was measured by Mettler DSC 30 with a heating rate of 2 K/min from −150 °C to +220 °C. The transition temperatures are peak values.

The 2D-WAXS experiments were performed by means of a rotating anode (Rigaku 18 kW) X-ray beam with a pinhole collimation and a two-dimensional Siemens detector. A double graphite monochromator for the Cu Kα radiation ($\lambda = 0.154$ nm) was used. A $\theta-\theta$ Siemens D500 Kristalloflex with a graphite-monochromatized Cu Kα X-ray beam was used for the investigation of the structure in the powder. The diffraction patterns were recorded in the 2θ range from 1 to 32° and are presented as functions of the scattering vector s; with $s = (2 \sin \theta)/\lambda$ where 2θ is the scattering angle. The number of stacked molecules in the isotropic phase was determined by assuming only nearest neighbor relations leading to the correlation distance of $d = 1.23/s_{max}$.[20] This value allows the average number of stacking molecules to be estimated, which form the aggregate as spherical units of volume $(\pi/6)d^3$ which is related to the molecular mass M by the following equation

$$\frac{\pi}{6}d^3 = \frac{Mn}{\rho N_A} \tag{1}$$

where n is the number of molecules, ρ is the assumed overall density of 1 g/cm^3, and N_A is Avogadro's number.

All MAS NMR experiments were performed on a Bruker Avance 700 spectrometer at a ^{1}H and ^{13}C Larmor frequencies of 700.1 and 176.0 MHz, using a standard double-resonance MAS probe supporting rotors of outer diameter 2.5 mm with spinning frequencies of 12.5 and 25 kHz. At high spinning frequency the additional heating effect caused by air friction becomes significant. Using the ^{119}Sn resonance of $Sm_2Sn_2O_7$ as a chemical shift thermometer, the correction term relative to the bearing gas temperature has been calibrated in a separate study.[21] All stated temperatures have been corrected by this procedure. For all samples, the initial 90° pulse length was 2.5 μs, and a recycle delay of 1 or 1.5 s was used. All dipolar recoupling experiments were carried out with equal excitation and reconversion times. The ^{1}H−^{1}H back-to-back (BABA) recoupling experiments[22] were performed using the excitation or recoupling sequences as described in ref 23. For the ^{1}H−^{13}C REREDOR spinning sideband patterns[24] two to eight full rotor periods were recorded in the indirect dimension, with the time increment set to 4.0 and 2.0 μs for 12.5 and 25 kHz, respectively. Prior to NMR experiments the samples were placed into the MAS rotors by filament extrusion.

The order parameter, S, is determined from residual ^{1}H−^{13}C dipole−dipole couplings according to $S = D_{exp}/D_{rigid}$, where D_{exp} is the experimentally measured ^{1}H−^{13}C dipolar coupling constant of a CH_n group and D_{rigid} is the reference ^{1}H−^{13}C coupling constant of the same moiety but in a totally rigid state. Hence, $S = 1.0$ stands for segments which are totally rigid on the time scale of the NMR experiment (i.e., ∼1 ms), excluding the fast rotation of methyl groups around their threefold symmetry axis. The higher its mobility (i.e., $S \rightarrow 0$), the broader the dynamic orientation distribution (i.e., $\Delta\theta \rightarrow 90°$); conversely, the lower its mobility (i.e., $S \rightarrow 1$), the narrower the orientation distribution (i.e., $\Delta\theta \rightarrow 0°$).

The PR-TRMC technique and method of data analysis as applied to discotic materials have been previously described in detail.[25] Briefly, solid samples in the form of powders are compressed into a Ka band (ca. 30 GHz) microwave cell. Uniform, micromolar concentrations of charge carriers are produced in the sample by a single 2−50 nanosecond pulse of 3 MeV electrons from a Van de Graaff accelerator. This method of ionization has the advantage that it does not perturb the primary or higher order molecular structure of the material as is the case for other procedures such as chemical doping. The amount of energy deposited in the sample, D J/m^3, is accurately known from dosimetry and the beam charge in the pulse which is routinely measured. If the charge carriers are mobile, microwaves propagating through the sample are attenuated, and this is monitored as a reduction in the microwave power reflected by the cell on irradiation. The change in conductivity per unit dose, $\Delta\sigma/D$, is derived from the change in microwave power, $\Delta P/P$, using the known sensitivity factor A.

$$\frac{\Delta P}{P} = -A\Delta\sigma \tag{2}$$

If the lifetime of the charge carriers is much longer than the pulse width, the sum of the one-dimensional, intracolumnar mobilities, $\sum\mu_{1D}$, can be calculated from the dose-normalized end-of-pulse conductivity according to

$$\sum\mu_{1D} = \frac{3E_p[\Delta\sigma_{eop}/D]}{W_{eop}} \tag{3}$$

In eq 3, E_p is the average energy absorbed in electronvolts per initial ionization event which is taken to be about 25 eV for the present materials. W_{eop} is the probability that the initially formed electrons and holes become localized on separate columnar stacks and do not decay within the pulse. The values of W_{eop}, which were close to 0.5, were calculated as described previously.[25b] A factor of 3 is included in eq 3 to take into account that the columnar stacks are randomly oriented in the samples studied. While the individual absolute values of the mobilities are subject to a ±25% error, the relative values should be accurate.

Acknowledgment. This work was financially supported by the EU project NAIMO Integrated Project No. NMP4-CT-2004-500355 and the Deutsche Forschungsgemeinschaft (Schwerpunktprogramm Organische Feldeffekttransistoren). M.K. thanks the Fonds der Chemischen Industrie and the Bundesministerium für Bildung und Forschung for financial support.

CM0602343

(20) Guinier, A. *X-ray Diffraction in Crystals, Imperfect Crystals, and Amorphous Bodies*; W. H. Freeman and Co.: San Francisco, CA, 1963.
(21) Langer, B.; Schell, I.; Spiess, H. W.; Grimmer, A.-R. *J. Magn. Reson.* **1999**, *138*, 182.
(22) Sommer, W.; Gottwald, J.; Spiess, H. W. *J. Magn. Reson.* **1995**, *A113*, 131.
(23) Feike, M.; Demco, D. E.; Graf, R.; Gottwald, J.; Hafner, S.; Spiess, H. W. *J. Magn. Reson.* **1996**, *A 122*, 214.
(24) Saalwächter, K.; Schnell, I. *Solid State Nucl. Magn. Reson.* **2002**, *22*, 154.
(25) Schouten, P. G.; Warman, J. M.; de Haas, M. P.; van Nostrum, C. F.; Gelinck, G. H.; Nolte, R. J.; Roeland, J. M.; Marc, M. J.; Zwicker, J. W.; Engel, M. K. *J. Am. Chem. Soc.* **1994**, *116*, 6880.